SPECIAL FEATURE: PERSPECTIVE

# First-principles–based reaction kinetics from reactive molecular dynamics simulations: Application to hydrogen peroxide decomposition

Daniil V. Ilyin[a], William A. Goddard III[a,1], Julius J. Oppenheim[a], and Tao Cheng[a]

Edited by Katepalli R. Sreenivasan, New York University, New York, NY, and approved August 14, 2018 (received for review December 20, 2017)

**This paper presents our vision of how to use in silico approaches to extract the reaction mechanisms and kinetic parameters for complex condensed-phase chemical processes that underlie important technologies ranging from combustion to chemical vapor deposition. The goal is to provide an analytic description of the detailed evolution of a complex chemical system from reactants through various intermediates to products, so that one could optimize the efficiency of the reactive processes to produce the desired products and avoid unwanted side products. We could start with quantum mechanics (QM) to ensure an accurate description; however, to obtain useful kinetics we need to average over ∼10-nm spatial scales for ∼1 ns, which is prohibitively impractical with QM. Instead, we use the reactive force field (ReaxFF) trained to fit QM to carry out the reactive molecular dynamics (RMD). We focus here on showing that it is practical to extract from such RMD the reaction mechanisms and kinetics information needed to describe the reactions analytically. This analytic description can then be used to incorporate the correct reaction chemistry from the QM/ReaxFF atomistic description into larger-scale simulations of ∼10 nm to micrometers to millimeters to meters using analytic approaches of computational fluid dynamics and/or continuum chemical dynamics. In the paper we lay out the strategy to extract the mechanisms and rate parameters automatically without the necessity of knowing any details of the chemistry. We consider this to be a proof of concept. We refer to the process as RMD2Kin (reactive molecular dynamics to kinetics) for the general approach and as ReaxMD2Kin (ReaxFF molecular dynamics to kinetics) for QM-ReaxFF–based reaction kinetics.**

reaction kinetics | ReaxFF reactive force field | reactive molecular dynamics | RMD2Kin | ReaxMD2Kin

Complex chemical processes underlie many important technologies, including combustion, propulsion, hydrocracking, fracking, chemical vapor deposition, atomic layer deposition, and reactive etching. Energy and environmental sustainability demands that we develop much more efficient processes with minimal energy cost and environmental impact. But the reactions taking place in these systems are far too complex to follow the details experimentally (1). Thus, the kinetics is usually greatly oversimplified in terms of straightforward reactive schemes that involve only a few of the reaction intermediates. Systems are often described using simple models with adjustable empirical parameters to characterize the coupling between temperature, overall reaction energetics, and time dependence of the energy release. This makes it difficult to connect real-world performance to the actual molecular species involved, and it is not necessarily clear what changes to make to the system to further optimize reaction conditions, fuels and oxidizers, and engine design to maximize power and efficiency while minimizing environmental impact. The necessary level of information usually cannot be obtained experimentally except maybe under very dilute conditions. Thus, another approach is needed.

[a]Materials and Process Simulation Center, California Institute of Technology, Pasadena, CA, 91125

Author contributions: D.V.I., W.A.G., and J.J.O. designed research; D.V.I., J.J.O., and T.C. performed research; D.V.I. and J.J.O. analyzed data; and D.V.I., W.A.G., and T.C. wrote the paper.

The authors declare no conflict of interest.

This article is a PNAS Direct Submission.



[1]To whom correspondence should be addressed. Email: wag@wag.caltech.edu.

This article contains supporting information online at www.pnas.org/lookup/suppl/doi:10.1073/pnas.1701383115/-/DCSupplemental.

Published online September 21, 2018.

We propose a paradigm, RMD2Kin (reactive molecular dynamics to kinetics), to describe computationally all of the details of the reaction kinetics, including rates, energetics, and mechanisms and to link macroscopic evolution of a chemical system to reaction details at the molecular scale that ultimately controls performance. We start by developing a reactive force field that provides the accuracy of first-principles quantum mechanics in describing the interatomic interactions of the reactive species in two-body calculations to enable reactive molecular dynamics (RMD) simulations at a fraction of the computational cost of QM. In the example here we used the reactive force field (ReaxFF) developed over the last 15 years to provide nearly the accuracy of QM. Using ReaxFF (denoted ReaxMD2Kin for ReaxFF molecular dynamics to kinetics), we report very detailed analysis of the system at the scale of 10 nm to understand the kinetics and mechanisms. We then extract analytic rate constant expressions that could be used in continuum simulations to describe phenomena at the 0.1–10-μm scales and could be averaged again to describe the system at the millimeter to centimeter scales found in the real world, e.g., in an engine. The atomistic simulations at the heart of this procedure may involve thousands to millions of atoms, depending on density, which would be impractical to describe solely with first-principles QM. We thus start with ReaxFF to mimic QM accuracy at the smallest two-body scale, so that the averaging for all higher scales is based on this QM starting point. This links the macroscopic performance of a particular system to individual reactions and permits testing a wide variety of systems to predict and optimize new formulations before experiment. This would allow synthesis and experiment to focus on the best possible systems, which could dramatically accelerate improvements in performance (2–19).

We illustrate the process here for a simple case of hydrogen peroxide decomposition. We analyze radical-initiated hydrogen peroxide decomposition and extract the mechanisms, rates, and transition-state enthalpies and entropies of the various reactions involved. We then use the extracted information to recreate the evolution of the system from initial concentrations. We show that the predicted concentrations reproduce well the observed concentrations, validating that our approach is self-consistent.

## The Reactive Force Field

ReaxFF (2) has the ability to describe surfaces, defects, diffusion, and chemical reactions, including formation and dissociation of chemical bonds to describe reactive processes in large-scale systems [millions of atoms (3) at nearly the accuracy of QM but at the computational cost of traditional classical force fields]. ReaxFF has been applied extensively to a number of reactive systems, which include hydrocarbons (2), nitramines (4), peroxides (5), aluminum metal and aluminum oxides (6, 7), silicon/silicon oxide interfaces (8) and dielectric breakdown (9), silicon carbides (10, 11), copper/nickel/cobalt interactions with carbon (12), magnesium and magnesium hydrides (13), lithium/lithium carbides (14), diamond-like carbon films and fullerene and bucky tube formation (12, 15–17), BiMoOx selective oxidation catalysts (18), the oxygen ion diffusion coefficient as a function of temperature in solid-state electrochemistry (19), and triple-phase electrochemical boundaries in Ni/YSZ/$H_2$ and Ni/YSZ/butane interfaces (20).

Important and relevant capabilities and characteristics of ReaxFF are as follows: (*i*) The ReaxFF charges have atomic-sized distribution (instead of being point charges, as in most other force fields), so that they properly include shielding of nearby atoms. This allows electrostatic interactions even on bonded atoms and avoids singularities that can occur with point charges. (*ii*) The charges are allowed to change dynamically as bonds are formed or broken and they operate between all atoms, not just nonbonded ones. (*iii*) Van der Waals (vdW) interactions are included between all atoms, not just nonbonded atoms. This allows the valence-bonding interaction to be monotonically attractive since the vdW inner wall balances the bond attraction. (*iv*) All valence interactions depend on the bond order, going to zero as the bonds are broken. (*v*) All parameters are obtained directly and systematically from QM, so we can extend them to all atoms of the periodic table.

We have recently combined ReaxFF with the polarizable QEq (PQEq) methodology (21, 22) to produce a polarizable ReaxFF (ReaxPQ) that captures self-consistently the local polarization needed for describing dielectric and magnetic properties. Our prototype of ReaxPQ has shown excellent description of reaction steps and polarization at reaction temperatures (23).

In this paper we validate our approach for the simple case of radical initiated hydrogen peroxide decomposition to form $H_2O$ and $O_2$ as final products. We start with reactants ($H_2O_2$ and OH) and allow them to react under various temperatures (*T*) and pressures (*P*) to form a series of intermediates (OH and $HO_2$ are prominent) to produce products ($H_2O$ and $O_2$). With no assumptions about the chemistry, the algorithm analyzes the molecules as they form and break bonds using the bond-order (BO) relationships from ReaxFF. We account for any complex intermediates and trace the dominant species back in time to the specific reactions that formed them. From this analysis we extract rate equations without any previous knowledge of the reaction kinetics. Then, using the derived reaction kinetics, we predict the overall evolution of the chemistry analytically, reproducing the details of the reaction kinetics observed in RMD.

We consider this paper to be a proof of concept, which is able to provide the same level of detail for far more complicated systems. By keeping track of the actual molecules formed as a function of time and then tracing them back in time, we can find the specific reaction responsible for any specific product and learn what the reactants were and what other products are formed. We thus obtain an unprecedented level of detail about the chemistry of a particular system, which we then can analyze or alter to meet the needs of the more significant problem.

## The Simulation System

The prototype system we use here to illustrate the process is enclosed in a periodic box 10 ×10 × 10 nm in size. At the start of the simulation, it is filled with 1,000 peroxide molecules at a density of 55 kg/$m^3$. The system geometry is minimized with the Polak–Ribiere conjugate gradient algorithm (24) and heated to a desired temperature (1,000–2,000 K in 100-K increments) by rescaling atom velocities with a Berendsen thermostat (25). To accelerate peroxide decomposition, the system is seeded by converting 20% (200) of the HOOH molecules into HO radicals randomly throughout the volume. Once the radicals are introduced, the system is allowed to react at constant number of atoms *N*, constant volume *V*, and constant energy *E*, denoted as *NVE*, for 200 ps at a time step of 1 fs. [Since the speed of sound is less than 1.82 nm/ps for liquid HOOH (1820 m/s at density 1400 kg/$m^3$) and the system is 10 nm wide at density 50 kg/$m^3$, the sound wave will take more than 5 ps to cross the system, and thus the local energy release from reactions will have a much more significant impact on the local temperature than will using a temperature bath. At

the same time, we show in *SI Appendix*, Fig. S3 that using isothermal dynamics at constant number of atoms $N$, constant volume $V$ and constant temperature $T$ ($NVT$) leads to comparable results.]

The simulations were run with LAMMPS (26) with the reax/c ReaxFF package (27). The input was prepared with Packmol (28). The 3D images and animations were prepared using Ovito (29). The raw data are available to interested researchers by request.

## Simulation Method

To analyze the RMD simulations, we must distinguish reactants and products from transient clusters that form and disappear without reacting due to interspecies collisions and bond vibrations. To define molecules, we analyze bonding interactions between all atoms at each time step and define bonds by setting bond-order cutoffs for the desired bonds (*SI Appendix*, Table S1). During vibrations, the bond lengths (and, therefore, bond orders) change as the molecule vibrates, so that, e.g., HOOH may seem to decompose to HO + OH but a few time steps later, the same atoms form an identical HOOH. We distinguish such redundancies from events where there is actually bond breaking or exchange of atoms by defining a time window (50 fs) during which a bond must remain below the bond-order cutoff to be considered broken.

The RMD simulation analysis yields a list of molecules present in the system at every time step. We analyze this information to define reactions at each timestep. By keeping track of all atoms that make up each molecule, we can go back in time and find which species reacted to give a particular product. We find that certain combinations of species may form long-lasting (>100 fs) metastable complex intermediates before reacting. The lifetimes of these intermediates depend on the collision geometry and rotational energy of the reactants. The intermediates are present in negligible concentration (no more than a few at a time in a box of 1000 molecules) and decompose with or without reacting. In order to account for the net reaction, we developed an algorithm that follows the life of the intermediate forward and backward in time until the initial reactants and final products only involve the dominant species. Then, we consider a reaction to be defined. This allows us to describe all reactions as interactions of the dominant species and to treat equivalent reactions in the same manner.

Once reactions are defined for each time step of the simulation, we analyze them to extract rate constants and barriers. For each given starting temperature, the overall concentration of all species changes throughout the simulation. Therefore, we split the time axis into 20 equal intervals in each of which the change in concentration has a small impact on the overall rate and then calculate the rate for each interval individually.

From the reaction trajectories, we know that the dynamics are quite complex. However, we find that most reactions can be described as two bodies (A and B) colliding to form two products (C and D), such as HOOH + OH → HOO + $H_2O$, or three products, such as HOOH + HOO → OH + $O_2$ + $H_2O$. For reactions that seem unimolecular (e.g., HOOH → HO + OH), we find that third bodies, M, play the role in energizing the reacting molecules without being modified. Thus, we can consider them implicitly in terms of $T$ and $P$ and account for their role with the rate constant.

For a bimolecular reaction that is first order in both reactants, A + B → C + D, the rate is given by $\mathfrak{R} = k[A][B]$, where the rate $\mathfrak{R}$ is the derivative of reaction concentration with time, $k$ is the rate constant, and [A] and [B] are concentrations of each reactant. We calculate $\mathfrak{R}$ as the ratio of the number of reactions in a time interval to the length of that interval and reactant concentrations [A] and [B] (or just [A] for unimolecular reactions) as the ratio of the number of reactants to the size of the simulation box. We obtain the overall rate constant for each temperature by solving the equation for $k$ in each time interval and averaging $k$ over all 20 intervals.

The Eyring equation explicitly relates the rate constant to temperature and to enthalpy and entropy of activation as

$$k = \frac{k_B T}{h}\, e^{\frac{\Delta S^{\ddagger}}{R}}\, e^{-\frac{\Delta H^{\ddagger}}{RT}}, \qquad [1]$$

where $k$ is the rate constant, $k_B$ is Boltzmann constant, $T$ is the temperature, $h$ is Planck constant, $R$ is the ideal gas constant, and ($\Delta H^{\ddagger}$) and ($\Delta S^{\ddagger}$) are the enthalpy and entropy of activation. Taking the logarithm and rearranging,

$$\ln\frac{k}{T} = -\frac{\Delta H^{\ddagger}}{R}\cdot\frac{1}{T} + \ln\frac{k_B}{h} + \frac{\Delta S^{\ddagger}}{R}. \qquad [2]$$

After computing $k$ as described above, we determine ($\Delta H^{\ddagger}$) and ($\Delta S^{\ddagger}$) by finding the least-squares fit of $\ln(k/T)$ vs. $1/T$. Then, using the calculated values for enthalpy and entropy of activation, we can analytically describe evolution of the chemistry. Specifically, we calculate rate constants at each temperature from the ($\Delta H^{\ddagger}$) and ($\Delta S^{\ddagger}$) in Eq. **1** at that temperature extracted from the fitted rate and compute the concentrations of all species from these rate constants for all dominant reactions. We find that these analytical predictions are consistent with our numerical data.

The ReaxMD2Kin method has a number of important parameters: temperatures, densities, initial concentrations, dominant species and reactions, and local concentrations, among others. In this illustration, we have set these parameters "by hand": We manually set the temperatures, densities, and initial concentrations; selected dominant species and reactions; and considered concentrations to be uniform throughout the system. For the target big-data problem of analyzing a system with a million atoms and hundreds of distinct reactions, this process would need to be automated. This presents a great opportunity to use machine learning. That is, a self-correcting algorithm based on the method described above would select optimum analysis parameters based on how well the analytical prediction reproduces the observed data. It thus would be trained to recognize dominant reactions, to follow complex pathways, to derive and analyze reaction mechanisms, and to ultimately provide an unprecedented level of detail about the chemistry of a particular complex system.

## Eyring/Arrhenius Parameters

The predicted reaction products as a function of time for the range of 1,000–2,000 K are shown in Fig. 1 and *SI Appendix*, Fig. S1. From analyzing the RMD, we find there are five dominant species (HOOH, $H_2O$, $O_2$, HOO, and OH) and seven dominant reactions. The rates as a function of time are plotted as $\ln(k/T)$ vs. $1/T$ for all seven dominant reactions in Fig. 2.

We use the dependence of concentration on time to compute rate constants for each reaction at each temperature. We fit the rate constants to the average system temperature using the Eyring equation, Eq. **1** to obtain ($\Delta H^{\ddagger}$) and ($\Delta S^{\ddagger}$) and also to calculate ($\Delta G^{\ddagger}_{300\,K}$) and ($\Delta G^{\ddagger}_{1,000\,K}$), listed in Table 1.

Then, using Eq. **1**, the system temperature, the initial concentrations, and the calculated ($\Delta H^{\ddagger}$) and ($\Delta S^{\ddagger}$), we analytically

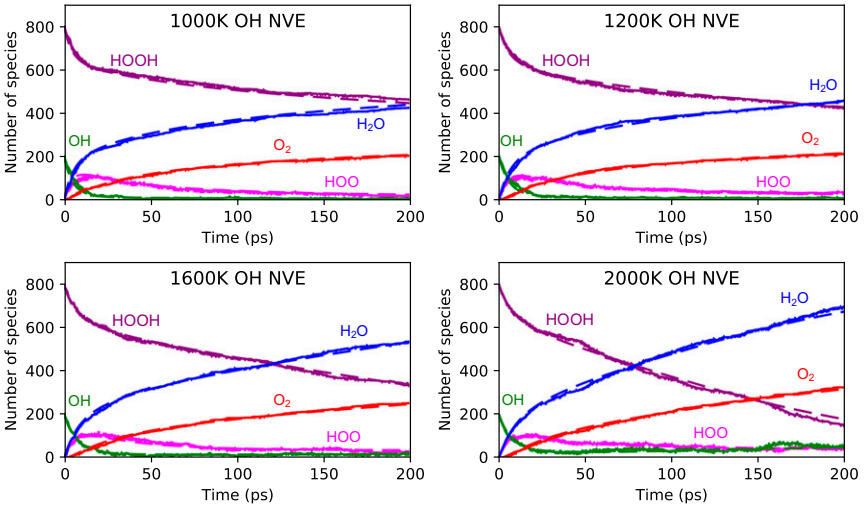


**Fig. 1. Observed (solid line) and predicted (dashed line) species as a function of time, for several temperatures from 1,000 K to 2,000 K (other temperatures are in *SI Appendix*, Fig. S1). Observed data are from the ReaxFF RMD; predicted data are the analytical extrapolation from initial concentrations using ($\Delta H^{\ddagger}$) and ($\Delta S^{\ddagger}$) determined from fitting rate constants to temperature.**

compute the expected concentrations of each dominant species as a function of time for all reactions. We find that these seven reactions describe the overall dynamics quite well, as shown in Fig. 1 and *SI Appendix*, Fig. S1, which compares the predicted and observed numbers of species present in each system throughout the simulation. We see very good agreement over the whole range of temperatures from 1,000 K to 2,000 K.

## Analysis of the Reactive Trajectories

All seven reactions have negative activation entropy. This is reasonable for all reactions except HOOH dissociation, where one would expect the transition state (TS) to be far looser than the reactant. We assume that it must have to do with a nonlinear increase in deactivating collisions as the temperature increases.

Four of the seven reactions have negative activation enthalpy, because they involve intrinsically unstable radicals for which the transition state provides a lower enthalpy than isolated reactants. Three of the reactions have positive activation enthalpy, because those reactants are more stable by themselves and thus have a lower enthalpy when isolated than when in the transition state. Specifically, for reaction 5, water is very stable, so even though a radical is present, the transition state has higher enthalpy than the reactants by themselves. For reaction 6, the only reactant is a neutral peroxide, so its transition state will naturally have higher enthalpy. Reaction 7 results in the formation of a rotationally bound metastable complex which has a significantly higher enthalpy in the transition state than the two OH radicals individually.

Reaction 1 is most important, since it initiates the reactions. Experimentally it is exothermic by ~29 kcal/mol at 300 K, but in our kinetics ($\Delta H^{\ddagger}$) = −4.89 kcal/mol and ($\Delta G^{\ddagger}_{300K}$) = −0.48 kcal/mol, indicating that not all of the exothermicity aids in getting to the TS. Indeed, the 3D reaction video (*SI Appendix*, Movie S1) and raw data show a considerable amount of rotational energy and our two-body QM and ReaxFF calculations find no TS.

Reaction 2 is exothermic by ~19 kcal/mol at 300 K, but ($\Delta H^{\ddagger}$) = −1.68 kcal/mol and ($\Delta G^{\ddagger}_{300\,K}$) = 3.27 kcal/mol. Our single-molecule

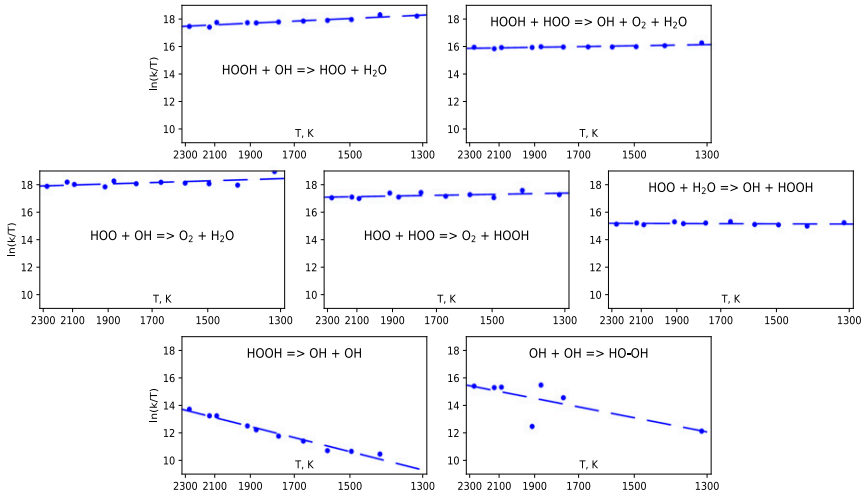


**Fig. 2. Calculated rate constants vs. average system temperature, extracted from the observed ReaxFF RMD and plotted as ln($k/T$) vs 1/$T$. The best least-squares linear fit to these data is shown (dashed line), which was used to determine the ($\Delta H^{\ddagger}$) and ($\Delta S^{\ddagger}$) for Eq. 1.**

**Table 1. Activation enthalpy (kcal/mol) and entropy (cal/mol-K) for the seven dominant reactions, calculated from a least-squares fit of the Eyring equation to the rate constants extracted from simulations at a range of temperatures from 1,000 K to 2,000 K.**

| Reaction no. | Reactions | $\Delta H^{\ddagger}$ kcal/mol | $\Delta S^{\ddagger}$ cal/mol-K | $\Delta G^{\ddagger}_{300K}$ kcal/mol | $\Delta G^{\ddagger}_{1,000K}$ kcal/mol |
|---|---|---|---|---|---|
| 1 | HOOH + OH → HOO + $H_2O$ | −4.89 | −14.7 | −0.48 | 9.81 |
| 2 | HOOH + HOO → OH + $O_2$ + $H_2O$ | −1.68 | −16.5 | 3.27 | 14.8 |
| 3 | HOO + OH → $O_2$ + $H_2O$ | −3.23 | −13.1 | 0.68 | 9.87 |
| 4 | HOO + HOO → $O_2$ + HOOH | −1.81 | −14.1 | 2.42 | 12.3 |
| 5 | HOO + $H_2O$ → OH + HOOH | 0.37 | −16.9 | 5.44 | 17.3 |
| 6 | HOOH → HO + OH | 25.9 | −8.75 | 28.5 | 34.7 |
| 7 | OH + OH → HO–OH | 20.1 | −7.78 | 22.4 | 27.9 |

QM and ReaxFF calculations find a barrier of 14 kcal/mol and 16 kcal/mol, respectively.

Reaction 3 is exothermic by ∼60 kcal/mol at 300 K, but ($\Delta H^{\ddagger}$) = −3.23 kcal/mol and ($\Delta G^{\ddagger}_{300\,K}$) = 0.68 kcal/mol, again indicating only a fraction of the exothermicity aids getting to the TS. Indeed, our QM and ReaxFF calculations find no TS.

Reaction 4 is exothermic by ∼40 kcal/mol at 300 K, but ($\Delta H^{\ddagger}$) = −1.81 kcal/mol and ($\Delta G^{\ddagger}_{300\,K}$) = 2.42 kcal/mol. Our QM and ReaxFF calculations find no TS.

Reaction 5 is endothermic by ∼29 kcal/mol at 300 K, but ($\Delta H^{\ddagger}$) = 0.37 kcal/mol and ($\Delta G^{\ddagger}_{300\,K}$) = 5.44 kcal/mol. Our QM and ReaxFF calculations for the reverse reaction find no TS.

Reaction 6 is endothermic by ∼50 kcal/mol at 300 K, but ($\Delta H^{\ddagger}$) = 25.9 kcal/mol and ($\Delta G^{\ddagger}_{300\,K}$) = 28.5 kcal/mol. Our QM and ReaxFF calculations for the reverse reaction find no TS. Of course many collisions with third bodies are necessary.

Two especially interesting cases are reaction 2 and reaction 7. For reaction 2, we found two common configurations of reactants: Fig. 3 *A* and *B*. These configurations differ in how the HOO radical attacks peroxide: If the H of HOO attacks the O of HOOH (Fig. 3*A*), then the H transfers to the peroxide O to form water and leaves behind $O_2$, while the peroxide O–O bond breaks and leaves behind OH. Thus, the products are $H_2O$, $O_2$, and OH. Thus reaction 2 is exothermic by ∼19 kcal/mol, but ($\Delta H^{\ddagger}$) = −1.68, a QM barrier of 14 kcal/mol (*SI Appendix*, Fig. S8). If, however, the O of HOO attacks the H of HOOH (Fig. 3*B*), then a metastable complex is formed in which the peroxide H gets transferred continually between HOOH and $HO_2$, with no net reaction (but half the time a transferred H). This metastable complex can live up to 1 ps, but may break up earlier due to interacting with a third body. This is illustrated in the 3D reaction videos, *SI Appendix*, Movies S2 and S3.

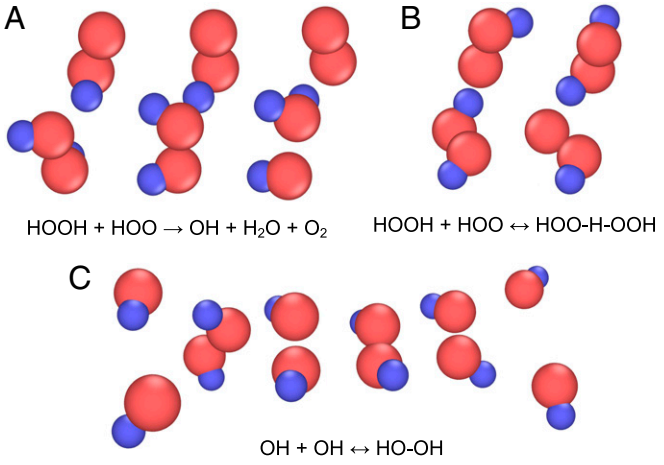


**Fig. 3. Reaction steps extracted from the ReaxFF reaction trajectories. (*A*) Reaction 2 of HOO and HOOH to produce OH, $O_2$, and $H_2O$. (*B*) Another collision geometry of HOO and HOOH resulting in a potential exchange of H between HOO and HOOH but no net reaction. (*C*) Reaction 7 showing the rotationally bound HO–OH complex that dissociates after hundreds of femtoseconds.**

Reaction 7 is interesting because it does not form stable HOOH. Instead, it forms a rotationally bound metastable HO–OH complex that lives for hundreds of femtoseconds and then dissociates back into OH + OH (Fig. 3*C*). This reaction therefore has a significant impact on the instantaneous concentration of OH and, due to the especially high reactivity of the OH radical, must be accounted for individually.

The kinetics for all seven reactions are fully dependent on kinetic processes in the condensed liquid, with behaviors quite different from those for a dilute gas. This shows the importance of describing the dynamics over hundreds of picoseconds while the reactions are occurring and provides unique and important information about the dynamics that is not available from low-pressure collisions or from QM calculations on the two-body interactions.

## Combustion-Induced Interface Instabilities

In the context of this special issue, we carried out atomistic simulations aimed at searching for chemically induced instabilities such as the Landau–Darrieus instability (LDI) (30). While it has been predicted that the flame front (considered as a fluid interface) should be unconditionally unstable, leading to the exponential growth of the interface perturbation (30), LDI has been a challenge to observe in experiments (31). The paradox has been resolved by accounting for the stabilizing influences of dissipation, diffusion, and finite front thickness on the interface dynamics at small scales (31). These mechanisms presume intense interactions and transports of many molecules at the kinetic and atomic scales (31). Theoretically, LDI requires an energy imbalance at the interface (32), which may be induced at the interface by energy fluctuations due to chemical reactions. Here, we consider the problem from the kinetic point of view, as the effect of chemical reactions on the front dynamics.

We examined a number of conditions with the goal of finding an instability. The shape of these systems was a long flat periodic box containing HOOH with a small partition at one end containing OH radicals, mixed in some cases with HOOH. At the interface between a region with HOOH seeded with OH and region of pure HOOH, we often saw some evidence for initiation of a plume developing into the HOOH, but it always dissipated before developing a clear instability. This is in line with the well-known

dissipative stabilization mechanisms of the Landau–Darrieus instability (26).

Specifically, we tried the following:

*i*) $10 \times 4 \times 25$-nm$^3$ box at 50 kg/m$^3$ density in both partitions; 20% OH.
*ii*) $10 \times 4 \times 25$-nm$^3$ box at 50 kg/m$^3$ density in both partitions; 100% OH.
*iii*) $40 \times 4 \times 100$-nm$^3$ box at 50 kg/m$^3$ density in both partitions; 20% OH.
*iv*) $40 \times 4 \times 100$-nm$^3$ box at 50 kg/m$^3$ density in both partitions; 100% OH.
*v*) $40 \times 4 \times 100$-nm$^3$ box at 50 kg/m$^3$ density in HOOH and 250 kg/m$^3$ in OH; 100% OH.
*vi*) $40 \times 4 \times 100$-nm$^3$ box at 1 kg/m$^3$ density in HOOH and 5 kg/m$^3$ in OH; 100% OH.
*vii*) $40 \times 0.4 \times 100$-nm$^3$ box at 50 kg/m$^3$ density in HOOH and 250 kg/m$^3$ in OH; 100% OH.
*viii*) $40 \times 0.4 \times 100$-nm$^3$ box at 1 kg/m$^3$ density in $H_2$ and $O_2$ and 5 kg/m$^3$ in OH; 100% OH.
*ix*) $20 \times 2 \times 10$-nm$^3$ box at 1,400 kg/m$^3$ equal density in HOOH and HOO; 5% HOO.

The box was selected to be flat in the *y* dimension to limit the evolution of the interface to two dimensions, with two extremely flat cases (one HOOH molecule thick) examined in systems *vii* and *viii*. In system *viii*, the HOOH reactant was changed to a stoichiometric ratio of dihydrogen and dioxygen to examine the effect of hotter radicals (H and O instead of HOO).

In all systems examined, the evolution of the instability was hindered. We hypothesize two main reasons for this.

First, the momentum that could potentially cause formation and propagation of a plume comes from small perturbations at the interface, i.e., the fast motion of individual OH radicals. These radicals are twice as small as the HOOH molecules with which they react, so that any radicals generated by the collision are expelled isotropically. Therefore, the initial momentum of the OH radicals is rapidly diminished within the first collisions, and the momentum of the perturbation disperses.

Second, the chemistry of the selected reactants and temperature range (1,000–2,000 K) is such that each reaction between the radical and reactant results in regeneration of just one radical. Therefore, the perturbation does not experience exponential growth, and the evolution of the interface is stable.

This is discussed further in *SI Appendix*, Fig. S4. We speculate that these issues might be solved by (*i*) selecting a geometry that provides a more focused forward momentum and (*ii*) selecting a chemistry that more easily yields a multiplication of radicals. For instance, by changing the reactants or parameters of the system to an extreme [e.g., replacing HOOH with hydrogen polyoxides, such as HOOOH or HOOOOH (33–35)] or using extremely high temperatures, we might see more radical multiplication that could lead to exponential growth of the plume.

## Summary and Conclusion

We illustrate here that QM-ReaxFF–based reaction kinetics (ReaxMD2Kin) can discover every reaction because every time a new product forms, we can go backward in time to determine exactly which reactants were involved (and how much energy they had, for a more sophisticated analysis) and then we can go forward to see what other products are formed in the same reaction (and how much internal energy they contribute, for a more sophisticated analysis). This allows us to discover minor products that we might want to eliminate or to maximize. To extract rate constants, we need to define concentrations and a length of time over which these concentrations are relatively constant. In the system examined here (a periodic cubic box of length 10 nm) we assume that all reactants are free to sample the whole box. For simulations on a much larger system we might have to consider diffusion lengths, but we anticipate that a system size of 10–20 nm (where the concentrations could be averaged) could be the right size to determine the fundamental reaction rates and mechanisms.

The particular case studied here of HOOH pyrolysis is interesting because none of the two-body reactions lead to a well-defined TS. Thus, to understand the kinetics, it is essential to follow the reactive dynamics over hundreds of picoseconds.

For more complex fuels such as gasoline, diesel, or JP10, we might have too many potential products to keep track of each individually, making it important to group by chemical functionality. This will be a fruitful area to apply machine-learning algorithms to group species appropriately and to refine the analyses automatically to ensure good statistics (36–39). As computers get faster and cheaper, these in silico methods should be applicable to wide ranges of reactive systems.

An important point to raise here is that the above discussions emphasize extending the spatial scale from hundreds of atoms to millions of atoms. However, this discussion did not deal with how to extend the timescale. There have been tremendous advances in methods to accelerate the dynamics sufficiently to capture in just 1 ns of QM molecular dynamics (MD) processes that would require timescales of microseconds or longer for ordinary MD. These methods have been applied to many reactive processes including full solvent QM studies of the oxygen reduction reaction for fuel cells (40) and the $CO_2$ reduction for environmental cleanup (41–43). Similar methods have been used to extend the timescales for MD using ordinary force fields up to microseconds and beyond while obtaining free energies for complex biological processes (44).

Indeed, we have prototyped one such method, adaptive accelerated ReaxFF reactive dynamics (aARRDyn) (45). This uses the BO concept in ReaxFF to dramatically accelerate the timescale when there are no broken bonds, while allowing normal RMD when bonds are broken. For the simple case of $H_2$ combustion (with just 100 molecules) aARRDyn was successful for describing the kinetics for timescales of 538 s using just 1.3 million time steps of dynamics. Optimization of such techniques for parallel and GPCU computing may help to move the timescales to multiple microseconds and maybe milliseconds in the near future.

## Acknowledgments

We thank Dr. Robert J. Nielsen (Smith), Dr. Sergey Zybin, Prof. Snezhana I. Abarzhi, and Aadyot Bhatnagar for helpful discussions. This work was supported by the US Department of Energy, Office of Energy Efficiency and Renewable Energy, Advanced Manufacturing Office Next Generation R&D Projects under Contract DE-AC07-05ID14517 (program manager Dickson Ozokwelu, in collaboration with Idaho National Laboratories, Rebecca Fushimi), by Office of Naval Research (Contract N00014-12-1-0538, Cliff Bedford and Chad A. Stoltz, program managers), and by the California Institute of Technology Toni and Bob Perpall and Ernest H Swift Summer Undergraduate Research Fellowships. This work was supported by resources provided by the Pawsey Supercomputing Centre with funding from the Australian Government and the Government of Western Australia through collaboration with Prof. Snezhana I. Abarzhi at the University of Western Australia. This work used the Extreme Science and Engineering Discovery Environment, which is supported by National Science Foundation Grant ACI-1548562.

1 Savard B, Bobbitt B, Blanquart G (2015) Structure of a high karlovitz $n$-$C_7H_{16}$ premixed turbulent flame. *Proc Combust Inst* 35:1377–1384.
2 van Duin ACT, Dasgupta S, Lorant F, Goddard WA (2001) ReaxFF: A reactive force field for hydrocarbons. *J Phys Chem A* 105:9396–9409.
3 An Q, et al. (2011) Elucidation of the dynamics for hot-spot initiation at nonuniform interfaces of highly shocked materials. *Phys Rev B* 84:220101.
4 Strachan A, van Duin ACT, Chakraborty D, Dasgupta S, Goddard WA (2003) Shock waves in high-energy materials: The initial chemical events in nitramine RDX. *Phys Rev Lett* 91:098301.
5 van Duin ACT, Zeiri Y, Dubnikova F, Kosloff R, Goddard WA (2005) Atomistic-scale simulations of the initial chemical events in the thermal initiation of triacetonetriperoxide. *J Am Chem Soc* 127:11053–11062.
6 Ojwang JGO, van Santen RA, Kramer GJ, van Duin ACT, Goddard WA, III (2009) Parametrization of a reactive force field for aluminum hydride. *J Chem Phys* 131:044501.
7 Ojwang JGO, van Santen R, Kramer GJ, van Duin ACT, Goddard WA, III (2008) Predictions of melting, crystallization, and local atomic arrangements of aluminum clusters using a reactive force field. *J Chem Phys* 129:244506.
8 van Duin ACT, et al. (2003) ReaxFFSiO reactive force field for silicon and silicon oxide systems. *J Phys Chem A* 107:3803–3811.
9 Tahir-Kheli J, Miyata M, Goddard W (2005) Dielectric breakdown in $SiO_2$ via electric field induced attached hydrogen defects. 14th Biennial Conference on Insulating Films on Semiconductors. *Microelectron Eng* 80:174–177.
10 Chenoweth K, Cheung S, van Duin ACT, Goddard WA, Kober EM (2005) Simulations on the thermal decomposition of a poly(dimethylsiloxane) polymer using the ReaxFF reactive force field. *J Am Chem Soc* 127:7192–7202.
11 Jaramillo-Botero A, Naserifar S, Goddard WA (2014) General multiobjective force field optimization framework, with application to reactive force fields for silicon carbide. *J Chem Theory Comput* 10:1426–1439.
12 Nielson KD, van Duin ACT, Oxgaard J, Deng WQ, Goddard WA (2005) Development of the ReaxFF reactive force field for describing transition metal catalyzed reactions, with application to the initial stages of the catalytic formation of carbon nanotubes. *J Phys Chem A* 109:493–499.
13 Cheung S, Deng WQ, van Duin ACT, Goddard WA (2005) ReaxFFMgH reactive force field for magnesium hydride systems. *J Phys Chem A* 109:851–859.
14 Han SS, van Duin ACT, Goddard WA, Lee HM (2005) Optimization and application of lithium parameters for the reactive force field, ReaxFF. *J Phys Chem A* 109:4575–4582.
15 Mueller JE, van Duin ACT, Goddard WA (2010) Competing, coverage-dependent decomposition pathways for $C_2H_y$ species on nickel (111). *J Phys Chem C* 114:20028–20041.
16 Mueller JE, van Duin ACT, Goddard WA (2009) Structures, energetics, and reaction barriers for $CH_x$ bound to the nickel (111) surface. *J Phys Chem C* 113:20290–20306.
17 Mueller JE, van Duin ACT, Goddard WA (2010) Development and validation of ReaxFF reactive force field for hydrocarbon chemistry catalyzed by nickel. *J Phys Chem C* 114:4939–4949.
18 Goddard WA, et al. (2006) Development of the ReaxFF reactive force field for mechanistic studies of catalytic selective oxidation processes on $BiMoO_x$. *Top Catal* 38:93–103.
19 van Duin ACT, Merinov BV, Jang SS, Goddard WA (2008) ReaxFF reactive force field for solid oxide fuel cell systems with application to oxygen ion transport in Yttria-stabilized zirconia. *J Phys Chem A* 112:3133–3140.
20 Sheng CY, Dean AM (2004) Importance of gas-phase kinetics within the anode channel of a solid-oxide fuel cell. *J Phys Chem A* 108:3772–3783.
21 Zhang Q, Cagin T, Goddard WA (2006) The ferroelectric and cubic phases in $BaTiO_3$ ferroelectrics are also antiferroelectric. *Proc Natl Acad Sci USA* 103:14695–14700.
22 Zhang Q, Goddard WA, III (2006) Charge and polarization distributions at the 90° domain wall in barium titanate ferroelectric. *Appl Phys Lett* 89:182903.
23 Naserifar S, Brooks DJ, Goddard WA, III, Cvicek V (2017) Polarizable charge equilibration model for predicting accurate electrostatic interactions in molecules and solids. *J Chem Phys* 146:124117.
24 Polyak B (1969) The conjugate gradient method in extremal problems. *USSR Comput Math Math Phys* 9:94–112.
25 Berendsen HJC, Postma JPM, van Gunsteren WF, DiNola A, Haak JR (1984) Molecular dynamics with coupling to an external bath. *J Chem Phys* 81:3684–3690.
26 Plimpton S (1995) Fast parallel algorithms for short-range molecular dynamics. *J Comp Phys* 117:1–19.
27 Aktulga HM, Fogarty JC, Pandit SA, Grama AY (2012) Parallel reactive molecular dynamics: Numerical methods and algorithmic techniques. *Parallel Comput* 38:245–259.
28 Martínez L, Andrade R, Birgin EG, Martínez JM (2009) Packmol: A package for building initial configurations for molecular dynamics simulations. *J Comput Chem* 30:2157–2164.
29 Stukowski A (2010) Visualization and analysis of atomistic simulation data with OVITO–the Open Visualization Tool. *Modelling Simul Mater Sci Eng* 18:015012.
30 Landau L (1988) On the theory of slow combustion. *Dynamics of Curved Fronts*, ed Pelcé P (Academic, San Diego), pp. 403–411.
31 Sivashinsky G (1983) Instabilities, pattern formation, and turbulence in flames. *Annu Rev Fluid Mech* 15:179–199.
32 Abarzhi SI, Ilyin DV, Goddard WA, Anisimov SI (2018) Interface dynamics: Mechanisms of stabilization and destabilization and structure of flow fields. *Proc Natl Acad Sci USA* 116:18218–18226.
33 Xu X, Goddard WA (2002) Peroxone chemistry: Formation of $H_2O_3$ and ring-$(HO_2)(HO_3)$ from $O_3/H_2O_2$. *Proc Natl Acad Sci USA* 99:15308–15312.
34 Xu X, Muller RP, Goddard WA (2002) The gas phase reaction of singlet dioxygen with water: A water-catalyzed mechanism. *Proc Natl Acad Sci USA* 99:3376–3381.
35 Datta D, Vaidehi N, Xu X, Goddard WA (2002) Mechanism for antibody catalysis of the oxidation of water by singlet dioxygen. *Proc Natl Acad Sci USA* 99:2636–2641.
36 Kim T, Yue Y, Taylor S, Matthews I (2015) A decision tree framework for spatiotemporal sequence prediction. *Proceedings of the 21th ACM SIGKDD International Conference on Knowledge Discovery and Data Mining, KDD '15*, eds Cao L, Zhang C (ACM, New York), pp. 577–586.
37 Lucey P, Bialkowski A, Carr P, Yue Y, Matthews I (2014) Presented by: "How to get an open shot": Analyzing team movement in basketball using tracking data. *MIT Sloan Sports Analytics Conference (SSAC)*, eds Gelman J, Morey D (MIT SSAC, MIT Press, Boston). Available at http://www.sloansportsconference.com/wp-content/uploads/2014/02/2014-SSAC-How-to-Get-an-Open-Shot.pdf. Accessed September 1, 2018.
38 Yue Y, Lucey P, Carr P, Bialkowski A, Matthews I (2014) Learning fine-grained spatial models for dynamic sports play prediction. *2014 IEEE International Conference on Data Mining*, eds Kumar R, Toivonnen H, Pei J, Huang JZ, Wu X (Conference Publishing Services, Los Alamitos, CA), pp. 670–679.
39 Ross S, Zhou J, Yue Y, Dey D, Bagnell JA (2013) Learning policies for contextual submodular prediction. *Proceedings of the 30th International Conference on International Conference on Machine Learning-ICML'13* (JMLR.org), eds Dasgupta S, McAllester D (MIT Press, Boston), pp. II-1364–III-1372.
40 Cheng T, et al. (2017) Mechanism and kinetics of the electrocatalytic reaction responsible for the high cost of hydrogen fuel cells. *Phys Chem Chem Phys* 19:2666–2673.
41 Cheng T, Xiao H, Goddard WA (2016) Reaction mechanisms for the electrochemical reduction of $Co_2$ to Co and formate on the Cu(100) surface at 298 K from quantum mechanics free energy calculations with explicit water. *J Am Chem Soc* 138:13802–13805.
42 Cheng T, Xiao H, Goddard WA (2017) Full atomistic reaction mechanism with kinetics for Co reduction on Cu(100) from ab initio molecular dynamics free-energy calculations at 298 K. *Proc Natl Acad Sci USA* 114:1795–1800.
43 Xiao H, Cheng T, Goddard WA, Sundararaman R (2016) Mechanistic explanation of the pH dependence and onset potentials for hydrocarbon products from electrochemical reduction of CO on Cu (111). *J Am Chem Soc* 138:483–486.
44 Markwick PRL, Pierce LCT, Goodin DB, McCammon JA (2011) Adaptive accelerated molecular dynamics (Ad-AMD) revealing the molecular plasticity of P450cam. *J Phys Chem Lett* 2:158–164.
45 Cheng T, Jaramillo-Botero A, Goddard WA, Sun H (2014) Adaptive accelerated ReaxFF reactive dynamics with validation from simulating hydrogen combustion. *J Am Chem Soc* 136:9434–9442.